CrystEngComm

PAPER

View Article Online
View Journal | View Issue

Cite this: *CrystEngComm*, 2015, **17**, 1871

In situ generation of functionality in a reactive binicotinic-acid-based ligand for the design of multi-functional copper(II) complexes: syntheses, structures and properties†

Dongsheng Deng,[a] Hui Guo,[a] Guohui Kang,[ab] Lufang Ma,[a] Xu He[a] and Baoming Ji*[a]

Received 6th November 2014,
Accepted 9th January 2015

DOI: 10.1039/c4ce02204a

www.rsc.org/crystengcomm

Under hydrothermal conditions, including tuning the reaction ratio and reaction temperature, three-dimensional (3D) porous {[Cu_3(hbpdc)$(OH)_2(H_2O)$]·$2H_2O$} (**1**), two-dimensional (2D) sheet {Cu_2(hbpdc)-$(H_2O)_2$}$_n$ (**2**), dinuclear [Cu(hbpdc)$_{0.5}(H_2O)_2$] (**3**), dimer [Cu_2(mbpdc)$_2$(py)$_2$]·$9H_2O$ (**4**), and mononuclear [Cu(hbpdcH_2)$(H_2O)_2$] (**5**) have been synthesized *via in situ* ligand transformation reaction, in which 3,3′-dimethoxy-2,2-bipyridine-6,6′dicarboxylic acid (mbpdcH_2) undergoes demethylation to 3,3′-dihydroxy-2,2′ bipyridine-6,6′-dicarboxylic acid (hbpdcH_4). The detailed coordination patterns of the hbpdcH_4 ligand have been revealed by single-crystal X-ray diffraction. The catalytic results demonstrate that polymers **1** and **2** can function as heterogeneous and reusable catalysts for the Strecker reaction of various imines. In addition, magnetic susceptibility measurements of complexes **1**, **2** and **4** reveal antiferromagnetic coupling between the copper(II) ions. Complex **1** follows the Curie–Weiss law, while **2** and **4** obey the Bleaney–Bowers dinuclear model.

Introduction

As a flourishing research field, metal–organic hybrid materials (MOHMs), containing paramagnetic metal ions incorporated into coordination polymers to fabricate extended structures, are currently of significant interest in materials chemistry, not only because of their fascinating structural diversities, but also their useful properties and promising application in the fields of gas storage, separation, magnetism, and catalysis.[1] In general, such MOHMs are typically composed of organic ligands as linkers and metal ions or metal ion clusters as nodes.[2] The assembly of reaction components from solution to the solid state can be achieved through various means, and each of these pathways can afford unique materials. In this respect, much effort has been directed toward developing the ability to control the reactions so that the products can be engineered to have the desired properties.[3] Although remarkable progress in this area has been achieved, the rational design and synthesis of MOHMs with unique structure and function still remain a significant challenge. Many factors, such as the nature of the metal ion,[4] structural features of the organic ligand,[5] counterions,[6] temperature,[7] reagent ratio,[8] pH value,[9] *etc.*, can exert great impact on the final architectures. With respect to temperature, its effect on the formation of the coordination polymers has not been intensively explored, although some reports described how the reaction temperature affects the generation of different coordination polymers.[7,10]

Currently, multidenate N- and O-donor bridging ligands have been widely used to construct MOHMs, due to their wide range of binding modes that provide superexchange pathways for magnetic coupling among paramagnetic metal centers.[11,12] Thus, inorganic–organic hybrid materials formed with pyridine-, pyrazine-, pyrimidine-, imidazole-carboxylic acid, *etc.* as linkers are known in the literature.[13] In this regard, binicotinic acid and its derivatives are excellent candidates for the construction of novel intriguing structures and topologies, because they have multiple coordination sites and can adopt more versatile conformations.[14,15]

In addition to magnetic properties, inorganic–organic hybrid materials have provided a tunable platform for the design of heterogeneous catalysts due to their high surface areas inside the pores and uniform catalytic sites (both metal ions and linkers can act as catalytic sites).[1c,16] Some MOHMs

[a] *College of Chemistry and Chemical Engineering, Luoyang Normal University, Luoyang 471022, PR China*
[b] *College of Chemistry and Chemical Engineering, Zhengzhou University, Zhengzhou 450052, PR China*

† Electronic supplementary information (ESI) available: X-ray crystallographic data for complexes **1–5** in CIF format, PXRD patterns, TGA plots, tables for hydrogen bonds, and NMR spectra. CCDC 968444–968449. For ESI and crystallographic data in CIF or other electronic format see DOI: 10.1039/c4ce02204a

have open metal sites which exhibit Lewis acidity and could catalyze organic reactions such as cyanosilylation of aldehydes or ketones, Mukaiyama aldol reaction, ring-opening of epoxides, Friedel–Crafts alkylation reaction, *etc.*[17]

In light of the abovementioned facts, we are here to focus our attention on using 3,3′-dimethoxy-2,2-bipyridine-6,6′dicarboxylic acid as a multidentate ligand to construct functional materials, based on the following considerations: 1) the two carboxylic hydrogen atoms can be easily deprotonated, allowing the four carboxylate oxygen atoms to bind to two or three or four metal centers, as observed in other binicotinic acid ligands;[14,15] and 2) when two methoxy groups hydrolyzed to hydroxyl groups through an *in situ* ligand transformation reaction under hydrothermal conditions, the resulting 3,3′-dihydroxy-2,2′bipyridine-6,6′-dicarboxylic acid ligand displays multidenate coordination modes, as depicted in Scheme 1a–f. The carboxylate oxygen can form a chelating bond to a metal center with the adjacent hydroxyl oxygen and pyridyl nitrogen. Consequently, the $hbpdc^{4-}$ ligand, with multifunctional coordination sites, is an effective component in the design of a diverse range of functional coordination complexes. On the basis of the above analysis, we first synthesized a 3D porous MOF, $\{[Cu_3(hbpdc)(OH)_2(H_2O)]\cdot 2H_2O\}$ (**1**).[14d] Next, we synthesized another four complexes $\{Cu_2(hbpdc)(H_2O)_2\}_n$ (**2**), $[Cu(hbpdc)_{0.5}(H_2O)_2]$ (**3**), $[Cu_2(mbpdc)_2(py)_2]\cdot 9H_2O$ (**4**), and $[Cu(hbpdcH_2)(H_2O)_2]$ (**5**) by using the $mbpdcH_2$ ligand with the help of different reaction conditions including reaction temperature and reactant ratio. The crystal structures and coordination modes of $hbpdcH_4$, along with the regulatory effect of reaction conditions on these complexes, have been analyzed. The magnetic properties of complexes **1**, **2** and **4** have been investigated. In addition, the heterogeneous catalytic activities of complexes **1** and **2** for the Strecker reactions of various imines in aqueous media have also been investigated.

Experimental section

Materials and general methods

The reagents needed for synthesis were used as received. 3,3′-Dimethoxy-2,2-bipyridine-6,6′dicarboxylic acid was prepared according to the literature method.[14d] C, H, and N microanalyses were carried out using a Flash 2000 elemental analyzer. IR spectra were recorded as KBr pellets on a Nicolet Avatar-360 spectrometer in the 4000–400 cm^{-1} range. TG-DSC measurements were performed by heating the crystalline sample from 25 to 900 °C at a rate of 2 °C min^{-1} in a N_2 atmosphere using a SDTQ600 differential thermal analyzer. Powder X-ray diffraction was performed with a Bruker D8-ADVANCE X-ray diffratometer operated using a 0.02° step scan from 5 to 50 °C in 2θ and 0.2 s preset time. ^1H NMR spectra were recorded on a Bruker DPX-400 spectrometer in $CDCl_3$ with TMS as an internal standard. Variable-temperature magnetic susceptibilities were measured with an MPMS-7 SQUID magnetometer. Diamagnetic corrections were performed with Pascal's constants for all constituent atoms.

Synthesis of polymer 1 ($\{[Cu_3(hbpdc)(OH)_2(H_2O)]\cdot 2H_2O\}_n$). Polymer **1** was prepared according to the literature method.[14d] A total of 0.2 mmol (63.5 mg) of $mbpdcH_2$ and 0.4 mmol (79.9 mg) of $Cu(CH_3COO)_2\cdot 4H_2O$ in a molar ratio of 1 : 2 were combined with 13 mL of deionized water in a 15 mL stainless steel bomb. This was sealed and heated at 160 °C for 4 days, then cooled to room temperature at a rate of 5 °C h^{-1}. Blue block crystals suitable for X-ray single crystal analysis were obtained in 81% yield (based on Cu). These crystals were separated, washed with water, and dried under ambient conditions.

Synthesis of polymer 2 ($\{Cu_2(hbpdc)(H_2O)_2\}_n$). Polymer **2** was obtained by the same method as that of **1** except that the reaction temperature was changed from 160 to 140 °C. After being cooled to room temperature, blue crystals were obtained in 85% yield. Anal. calcd. for $C_{12}H_8Cu_2N_2O_8$: C, 33.11; H, 1.85; N, 6.44%. Found: C, 33.18; H, 1.96; N, 6.49%. IR (KBr, cm^{-1}): 3416(s), 3138(m), 1651(m), 1576(s), 1424(m), 1362(s), 1318(m), 1120(m), 877(m), 863(m), 797(s), 699(s).

Synthesis of complex 3 ($[Cu(hbpdc)_{0.5}(H_2O)_2]$). Complex **2** was synthesized by the same procedure used for preparing **1** except that the metal-to-ligand ratio was altered from 1 : 2 to 2 : 1. After being cooled to room temperature, blue crystals were obtained in 20% yield. Anal. calcd. for $C_6H_6CuNO_5$: C, 30.58; H, 2.57; N, 5.94%. Found: C, 30.66; H, 2.69; N, 5.99%. IR (KBr, cm^{-1}): 3418(m), 3041(s), 2950(m), 1697(s), 1634(s), 1567(m), 1492(m), 1422(s), 1359(s), 1289(s), 1242(m), 1172(m), 912(s), 863(s), 851(m), 790(s), 715(m).

Synthesis of complex 4 ($[Cu_2(mbpdc)_2(py)_2]\cdot 9H_2O$). Complex **4** was prepared by a similar procedure to that for **1** except

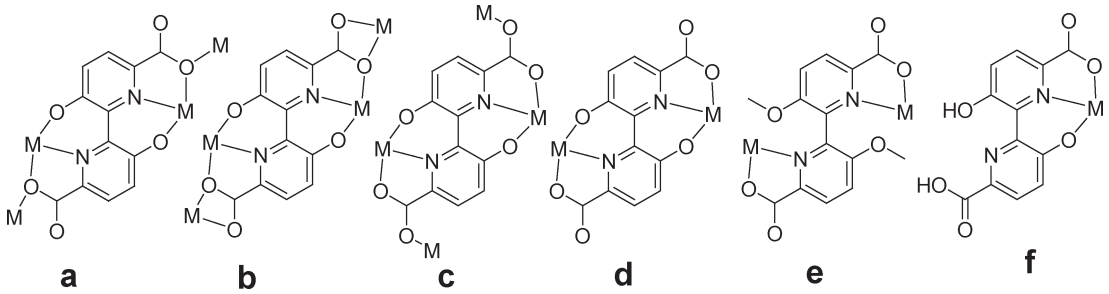

Scheme 1 The coordination modes of the $hbpdcH_4$ ligand in complexes **1**–**5**.

that the metal-to-ligand ratio was altered from 1 : 2 to 1 : 1, and pyridine was used as the additive. After being cooled to room temperature, blue crystals were obtained in 70% yield. Anal. calcd. for $C_{38}H_{48}Cu_2N_6O_{21}$: C, 43.39; H, 4.60; N, 7.99%. Found: C, 43.52; H, 4.72; N, 8.15%. IR (KBr, cm^{-1}): 3453(m), 2965(w), 2933(w), 2863(w), 1639(s), 1568(m), 1429(s), 1389(s), 1337(m), 1225(m), 1124(m), 893(m), 854(m), 788(m), 709(m).

Synthesis of complex 5 ([Cu(hbpdcH$_2$)(H$_2$O)$_2$]). The preparation of 5 was similar to that of 1 except that the metal-to-ligand ratio was altered from 1 : 2 to 1 : 1. After being cooled to room temperature, blue crystals were obtained in 70% yield. Anal. calcd. for $C_{12}H_{10}CuN_2O_8$: C, 38.56; H, 2.70; N, 7.49%. Found: C, 38.69; H, 2.86; N, 7.62%. IR (KBr, cm^{-1}): 3418(w), 3041(s), 2950(m), 1697(s), 1634(s), 1567(m), 1492(m), 1422(s), 1359(s), 1289(s), 1242(m), 1172(m), 912(s), 863(s), 851(m), 790(s), 715(m).

Single-crystal structure determination

A suitable single crystal was carefully selected under a polarizing microscope and glued carefully to a thin glass fiber. Crystallographic data for 1–5 were collected on a Bruker Smart Apex-II CCD area detector equipped with graphite-monochromatic Mo Kα radiation (λ = 0.71073 Å) at room temperature. Data were reduced using SAINTPLUS, and an empirical absorption correction was applied using the SADABS program. The structures were solved with direct methods and refined with full-matrix least-squares techniques on F^2 using the SHELXTL program package.[18,19] The non-hydrogen atoms were placed in geometrically ideal positions and refined as riding atoms with a common isotropic thermal parameter. Details of the structure solution and final refinements are given in Table 1. CCDC 96844 (1), 968446 (2), 968447 (3), 968448 (4) and 968449 (5) contain the supplementary crystallographic data.

Catalysis experiments

Polymers 1 and 2 were activated at 120 °C for 8 h under vacuum before the reaction was carried out. A typical Strecker reaction procedure was performed as follows. A quantity of 24 mg (0.005 mmol of 1) of the catalyst was suspended in dry CH_2Cl_2 (2 mL) followed by the addition of imines (0.1 mmol) and trimethylsilyl cyanide (0.15 mmol). The reaction mixtures were stirred for 4 h at 298 K under N_2. Catalytic recyclability was checked four times with the same batch of the catalyst. The recovered catalysts were characterized by X-ray powder diffraction and showed identical results to those of the fresh samples.

Results and discussion

Synthesis and spectroscopic characterization

As it is well known, *in situ* ligand transformation reaction may occur during hydrothermal reaction, which is currently regarded as an effective strategy to obtain novel MOHMs that are inaccessible or not easily achieved by conventional methods.[20] However, the controlled synthesis of MOHMs is still a major challenge.[21] Small changes in one or more of the variables of hydrothermal reaction, such as temperature, metal-to-ligand ratio, and pH value, have a profound influence on the final crystallization outcome.[22] As far as these factors are concerned, complexes 1–5 were successfully obtained by the *in situ* reaction of mbpdcH$_2$ with Cu(II) acetate through tuning hydrothermal temperature, metal-to-ligand ratio and additive. The self-assembly strategies are given in Scheme 2. On the basis of identical reactants, the structures of 1 and 2 differed in the case of altered reaction temperature. Complexes 3 and 5 were obtained by changing the metal-to-ligand ratio. Finally, complex 4 can be obtained by altering the metal-to-ligand ratio in the addition of pyridine.

Table 1 Crystallographic data and structure refinement summary for complexes 1–5

Complexes	1	2	3	4	5
Chemical formula	$C_{12}H_{10}Cu_3N_2O_{10}$	$C_{12}H_8Cu_2N_2O_8$	$C_6H_6CuNO_5$	$C_{38}H_{48}Cu_2N_6O_{21}$	$C_{12}H_{10}CuN_2O_8$
Formula weight	532.84	435.28	235.66	1051.90	373.76
Crystal system	Monoclinic	Monoclinic	Triclinic	Triclinic	Triclinic
Space group	$C2/c$	$P2_1/c$	$\bar{P}1$	$\bar{P}1$	$\bar{P}1$
a/Å	16.892(3)	18.211(3)	6.2937(16)	12.1868(13)	4.785(7)
b/Å	15.722(2)	5.1283(10)	6.8393(17)	12.4222(13)	9.330(14)
c/Å	5.8595(9)	13.915(3)	9.545(4)	15.4307(16)	14.53(2)
α/°	90	90	99.689(4)	77.399(10)	89.807(16)
β/°	106.112(2)	96.803(2)	90.764(4)	88.583(10)	81.067(16)
γ/°	90	90	116.946(3)	85.884(10)	77.496(16)
Volume/Å^3	1495.0(4)	1290.4(4)	359.14(19)	2273.8(4)	625.4(16)
Z	4	4	1	2	2
D_{calc}/g cm^{-3}	2.367	2.241	2.179	1.536	1.985
μ/mm^{-1}	4.294	3.348	3.027	2.274	1.798
T/K	293(2)	294(2)	293(2)	291(2)	296(2)
Reflns. collected	5230	8900	2762	17 105	4758
Unique reflns	1388	2395	1333	8423	2309
R_{int}	0.0272	0.0295	0.0215	0.0265	0.0203
Goodness-of-fit	1.029	1.022	1.073	1.030	1.058
R_1 ($I > 2\sigma$)	0.0244	0.0296	0.0338	0.0395	0.0282
wR_2 ($I > 2\sigma$)	0.0611	0.0724	0.0813	0.0981	0.0750

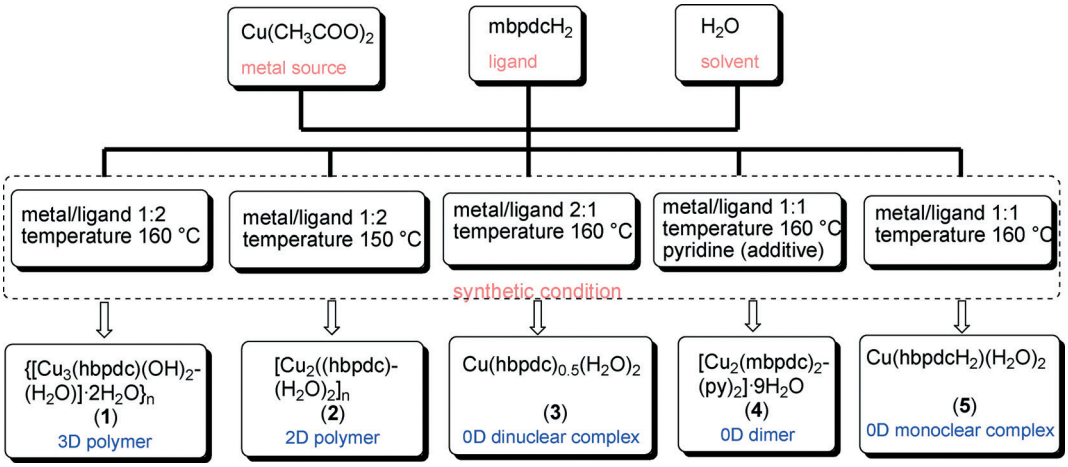

Scheme 2 Self-assembly syntheses of **1**–**5**.

Description of crystal structures

Crystal structure of 1. Under 160 °C hydrothermal conditions, the reaction of Cu(II) acetate with the $mbpdcH_2$ ligand can afford polymer **1** with a metal-to-ligand ratio of 2 : 1. Polymer **1** features a highly ordered 3D nanoporous structure encapsulating a zigzag water chain. The detailed structural discussion of **1** has been reported in our previous paper.[14d]

Crystal structure of 2. The asymmetric unit consists of two crystallographically unique Cu(II) ions, two halves of $hbpdc^{4-}$ ligands, and two coordinated water molecules. The Cu1 and Cu2 ions lie on general positions while the two halves of $hbpdc^{4-}$ lie on another independent inversion center. The coordinated water molecules also occupy general positions. As shown in Fig. 1a, the coordination geometry of the Cu1 ion can be described as a distorted square-pyramidal geometry, being bonded to two carboxylate oxygen atoms from one $hbpdc^{4-}$ ligand (Cu–O 1.865(2) and 1.941(2) Å), one nitrogen atom of the $hbpdc^{4-}$ ligand (Cu–N 1.985(3) Å) and two aqua ligands (Cu–O 1.973(2) and 2.273(3) Å) (Table S1, in the ESI†). The Cu2 ion adopts a six-coordinated octahedral geometry. The equatorial plane is composed of two chelating carboxylate oxygen atoms, one monodentate carboxylate oxygen atom, and the monodentate nitrogen atom of two $hbpdc^{4-}$ ligands. The apical positions are occupied by the monodentate carboxylate oxygen atoms of the $hbpdc^{4-}$ ligand. The O–Cu–O and O–Cu–N angles in the equatorial plane and the O–Cu–O angle along the apical direction are in the range of 85.62(10)–173.41(11)° (Table S1, in the ESI†), indicating that the octahedron is very distorted.

In the crystal structure, one $hbpdc^{4-}$ ligand in a bis-(tridentate) chelating mode connects Cu1 and Cu1A, giving a dinuclear copper building block $[Cu_2N_2O_2(CO_2R)_2]$ with short separations of Cu1···Cu1 (6.212 Å), while the other $hbptc^{4-}$ ligand also in the bis-(tridentate) chelating mode links Cu2 and Cu2A, leading to the other dinuclear copper building block $[Cu_2N_2O_2(CO_2R)_2]$ with separations of Cu2···Cu2 (6.238 Å). The former $hbptc^{4-}$ ligands in a bidentate $(k^1\text{-}k^1)\text{-}(k^1\text{-}k^1)\text{-}\mu_2$ bridging mode (Scheme 1b) connect the two adjacent but different dinuclear copper building blocks, resulting in one dimensional chains along the *a* axis with a Cu1···Cu2 distance of 4.698 Å, as depicted in Fig. 1b. Additionally, it is noted that the latter $hbptc^{4-}$ ligands in the bidentate $(k^1)\text{-}(k^1)\text{-}\mu_2$ bridging mode (Scheme 1c) link the two adjacent $[Cu_2N_2O_2(CO_2R)_2]$ building blocks, resulting in one dimensional chains along the *b* axis with a Cu2···Cu2 distance of 5.128 Å, as depicted in Fig. 1c. The two kinds of chains are not parallel but form angles about 80° with each other. Therefore, the resulting two-dimensional sheet in the *ab* plane is formed by two kinds of chains sharing the Cu2 ions, as shown in Fig. 1d.

In addition, through other hydrogen-bonding interactions originating from the coordinated water hydrogen atom and the carboxyl oxygen atom between the adjacent sheets (O···O, 2.689(3) Å, 162.1°; 2.731(3) Å, 165.9°; 2.855(3) Å, 169.3°; 2.861(3) Å, 172.0°), the 2D sheet is further linked into a 3D supramolecular network, as shown in Fig. 1e. Details of hydrogen bond interactions are listed in Table S2 (see the ESI†).

Crystal structure of 3. X-ray single crystal analysis of **3** indicates a discrete centrosymmetric dinuclear complex, as shown in Fig. 2a. The asymmetric unit consists of one crystallographically unique Cu(II) ion, half $hbpdc^{4-}$ ligand, and two coordinated water molecules. The Cu(II) ion adopts a five-coordinated square-pyramidal geometry, formed by one nitrogen donor and two carboxylate oxygen atoms from one $hbptc^{4-}$ ligand and two aqua ligands. The Cu–N and Cu–O bond distances lie in the range of 1.980 Å and 1.861(3)–2.291(3) Å (Table S1, in the ESI†), being comparable to those found for similar complexes in the literature.[23] For each $hbpdc^{4-}$ ligand, two carboxylate groups take the same chelating coordination mode to join two Cu(II) ions (see Scheme 1d). As a result, each $hbpdc^{4-}$ ligand links two Cu(II) ions to form a dinuclear unit. Within this unit, the neighboring Cu1A···Cu1B separations are 3.854 Å.

In the crystal structure of **3**, the dinuclear units are connected to each other through the formation of hydrogen bonds between the adjacent coordinated water molecules, resulting in a 1D chain along the *c* axis. The adjacent chains

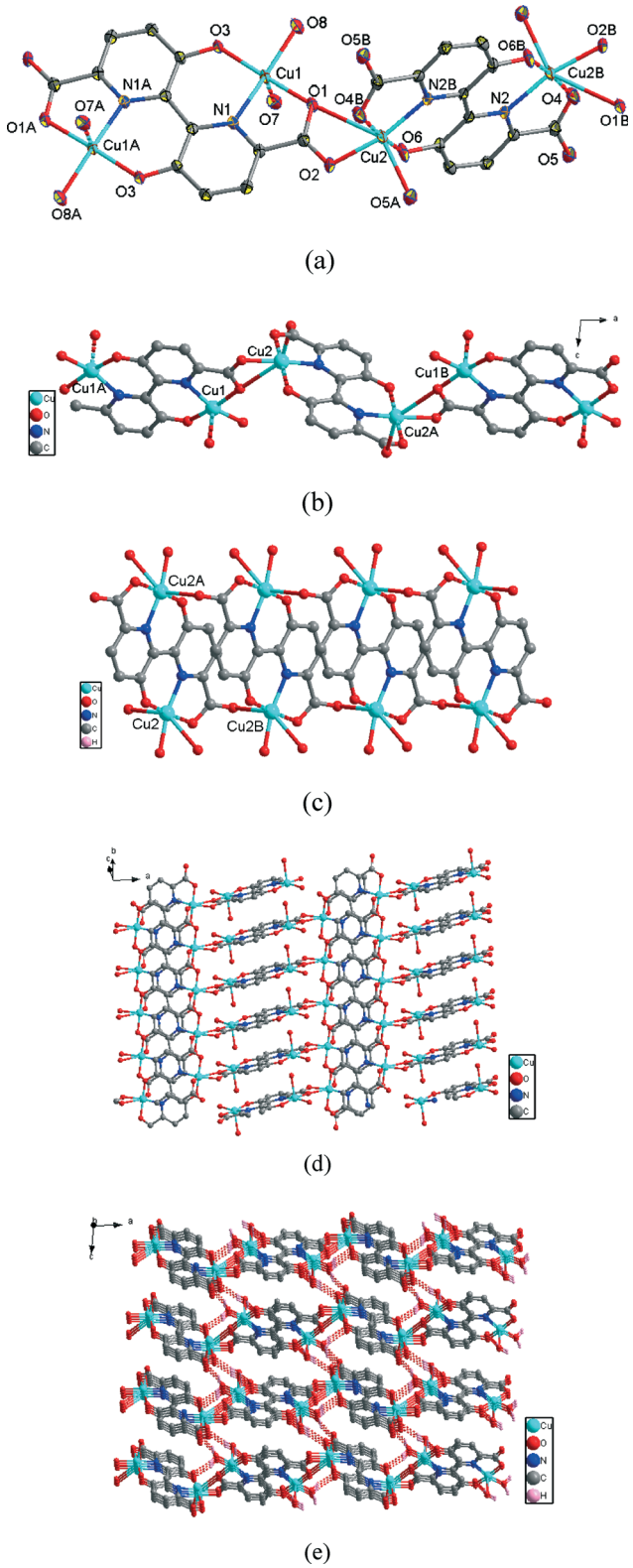

Fig. 1 (a) The coordination environment of the Cu(II) center in **2** with the ellipsoids drawn at the 50% probability level. The hydrogen atoms are omitted for clarity (the axial long Cu–O bonds are shown as broken lines). Symmetry operators: (A) $-x + 1, -y, -z + 1$; (B) $-x + 2, -y + 1, -z + 1$. (b) and (c) View of the 1-D chain in **2** (the axial long Cu–O bonds are shown as broken lines). (d) View of the 2-D sheet in the *ab* plane. (e) View of the 3-D supramolecular network. The extensive hydrogen bonds are colored red.

are further connected to each other through the formation of hydrogen bonds between water molecules and carboxylate oxygen atoms, resulting in a 3D supramolecular network, as shown in Fig. 2b. Details of hydrogen bond interactions are listed in Table S2 (see the ESI†).

Crystal structure of 4. In contrast to the above coordination polymers **1** and **2**, complex **4** is a discrete double-stranded dimer, which crystallizes in the monoclinic space group $P\bar{1}$, and each asymmetric unit consists of two Cu(II) ions, two $mhbptc^{2-}$, and nine lattice water molecules. As depicted in Fig. 3a, the structure of **4** is built up of dinuclear units, in which the two copper ions have the same coordination modes with Cu···Cu = 4.500(1) Å. Each Cu(II) ion shows a five-coordinated square-pyramidal geometry, formed by two nitrogen donors, two carboxylate oxygen atoms from two $mhbpdc^{2-}$ ligands and one pyridine nitrogen atom, in which the Cu–O bond distances range from 2.033(3) to 2.150(3) Å, and Cu–N bond distances lie in the normal range of 2.196(3)–2.212(3) Å (Table S1, in the ESI†). The two $mhbpdc^{2-}$ adopt bis(didentate) chelating fashions (Scheme 1e) to link two copper ions with the twist angles between two 2,2′-bipyridyl rings being 63.6(3) and 67.0(2)°, which are significantly larger than those found in complexes **1**–**3**.

Considering that there are nine lattice water molecules within the structure, the packing of complex **4** in the crystal lattice is worth mentioning. In the crystal structure of **4**, the crystalline water molecules and carboxylate oxygen atoms are the main part of the hydrogen bonded motifs. The lattice water molecules contribute to bridge the adjacent double-stranded dimers to a 3D network with hydrogen bonds, as shown in Fig. 3b. The water molecules are in the interlayer space and linked to each other by hydrogen bonds to form $(H_2O)_{14}$ clusters. Fig. 3c shows the five molecules (O4, O5, O7, O8 and O9) and their symmetric equivalents that form a ten-membered ring, which is further hydrogen bonded to a water tetramer (O2, O3, O1, O6), giving a $(H_2O)_{14}$ cluster, with a non-bonded O···O distance of 2.901 Å. Similar to that observed in the reported complexes,[24] both water–MOF and water–water interactions can be important for the stability of the overall 3D structure of **4**. Details of hydrogen bond interactions are listed in Table S2 (see the ESI†).

Crystal structure of 5. By reducing the ligand-to-metal ratio from 1 : 2 to 1 : 1, the reaction of copper ions with $mbpdcH_2$ produced the mononuclear complex **5**. It is held together through the formation of hydrogen bonds among mononuclear (rather than dinuclear) copper-$bpdcH_2$ units. The asymmetric unit consists of one crystallographically unique Cu(II) center, one $hbpdcH_2^{2-}$ ion, and two coordinated water molecules, as depicted in Fig. 4a. In **5**, the Cu(II) ion is also five-coordinated. Every Cu(II) ion binds simultaneously to one carboxylate oxygen, one hydroxyl oxgen and one pyridyl nitrogen from one $hbpdcH_2^{2-}$ ion and two aqua ligands.

In the crystal structure of **5**, the $hbpdcH_2^{2-}$ ion adopts a tridentate chelating fashion (Scheme 1f) to bind a Cu(II) ion through adjacent one carboxylate O6, one hydroxyl O1 and

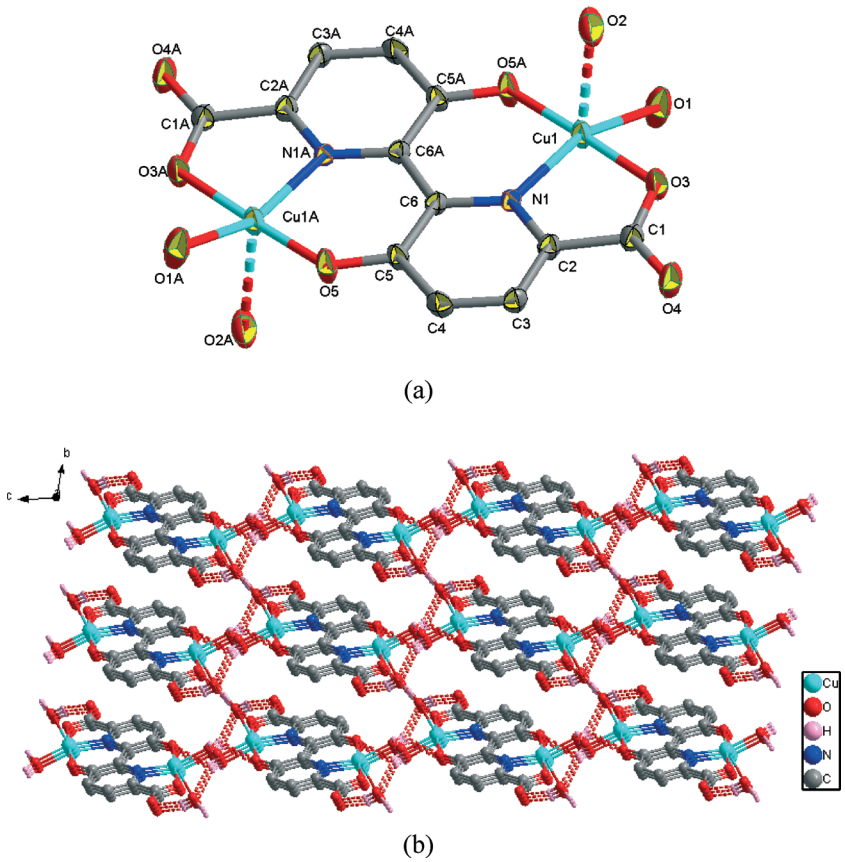

Fig. 2 (a) The coordination environment of the Cu(II) center in **3** with the ellipsoids drawn at the 50% probability level. The hydrogen atoms are omitted for clarity (the axial long Cu–O bonds are shown as broken lines). Symmetry operators: (A) $-x, -y + 1, -z + 2$. (b) View of the 3-D supramolecular network. The extensive hydrogen bonds are colored red.

one pyridine N2. The second carboxylic acid and hydroxyl functions remain uncoordinated and are unprotonated, thus neutralizing the overall positive charge of the Cu(II) ions. In the packing motif, each mononuclear unit is assembled *via* hydrogen bonding between carboxylic hydrogen and carboxylic oxygen together with the coordinated water molecules stabilizing the mononuclears which completely results in the overall 3D supramolecular structure of **5**, as shown in Fig. 4b. Details of hydrogen bond interactions are listed in Table S2 (see ESI†).

Thermal stability and powder X-Ray diffraction

The pure phases of complexes **1**, **2**, **4** and **5** were confirmed by PXRD measurements, and the results are shown in Fig. S1.† Meanwhile, each PXRD pattern of the as-synthesized sample is consistent with the simulated one. This result shows the phase purity of the bulk samples.

The thermal stabilities of **2**, **4** and **5** were examined by thermogravimetric analysis (TGA), and the results are shown in Fig. S2.†

Complexes **2** and **5** undergo weight losses of 8.79% and 9.76%, respectively, which can be assigned to the loss of coordinated water molecules (calcd. 8.27% for **2** and 9.63% for **5**), and the frameworks of **2** and **5** remain stable up to approximately 402 °C.

The TGA curve of **4** exhibits an initial weight loss from room temperature to 105 °C, with an observed weight loss of 15.7% corresponding to the release of lattice water molecules (calcd. 15.4%). After that an additional weight loss of 9.2% up to 293 °C may be attributed to the gradual release of coordinated pyridine molecules.

Catalytic activity

Earlier work revealed that some Cu-containing polymeric compounds were found to be good heterogeneous catalysts that offer the practical advantages of simplifying the separation and isolation of products and of the potential for catalyst recycling.[25] These results have prompted us to design new Cu-containing polymeric compounds as potential heterogeneous catalysts. The crystal structure analysis reveals that there are two structural novelties in Cu-MOFs, **1** and **2**. For example, both networks contain coordinatively unsaturated metal centers. In addition, the other unique feature is the observation that Cu(II) ions are coordinated by a large number of labile water molecules. These structural features encouraged us to explore possible organic transformations. As it is well known, the Strecker reaction is one of the preeminent multicomponent reactions useful for the synthesis of α-amino acids *via* the intermediacy of α-amino nitriles.[26]

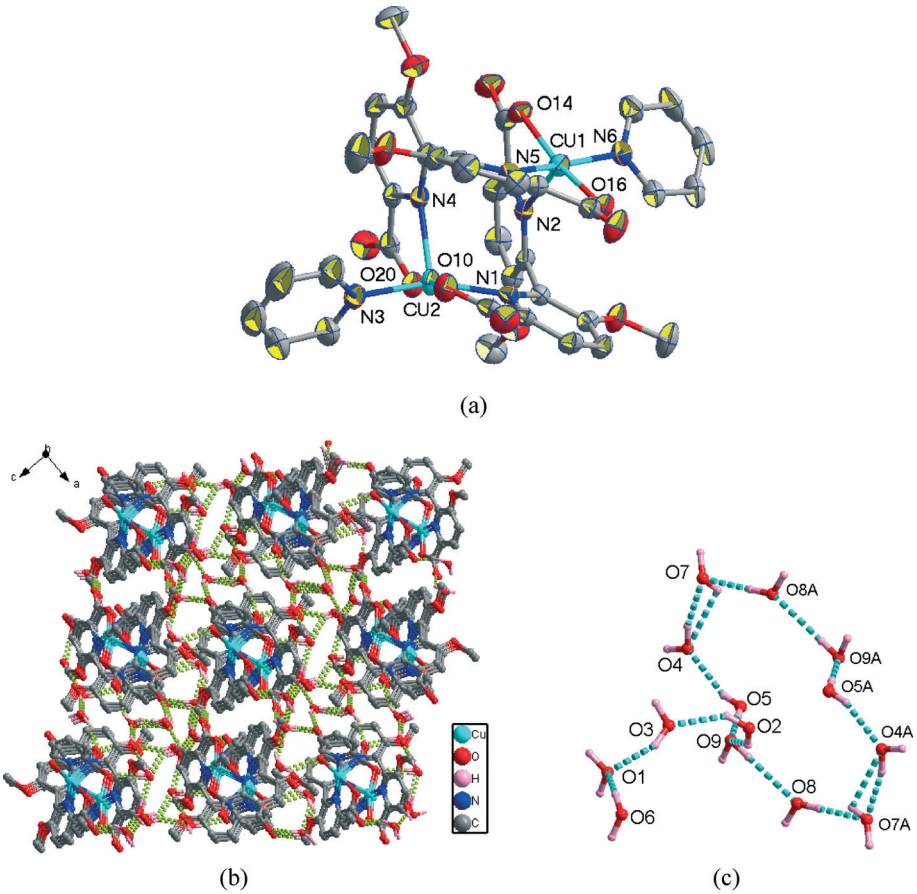

Fig. 3 (a) Coordination environment of the Cu ion in **4** with the ellipsoids drawn at the 50% probability level. The hydrogen atoms and lattice water are omitted for clarity. (b) View of the 3-D supramolecular network. The extensive hydrogen bonds are indicated as dotted lines. (c) View of the $(H_2O)_{14}$ cluster in **4** (hydrogen bonds are indicated as dotted lines).

Therefore, we examined their performance as heterogeneous catalysts for the Strecker reaction of imines under mild conditions.

To evaluate the catalytic activity of complexes **1** and **2**, these complexes were activated at 120 °C for 8 h under vacuum, to remove coordinated H_2O molecules before the reaction. Next, we used the trimethylsilyl cyanide addition to *N*-benzylidenebenzenamine as a test reaction (Table 2, entry 1) and afforded the corresponding α-amino nitrile as the principal product. In a typical reaction, a 24 mg (0.005 mmol) sample of **1** was used for the conversion of 0.1 mmol of imine in dry CH_2Cl_2 at room temperature. An excess of 50% trimethylsilyl cyanide was employed with respect to the amount of imine. The progress of the reaction was monitored by the thin layer chromatography. After the required reaction time, the resulting solution was filtered to remove the catalyst. The resulting solvents were evaporated in vacuum, and aqueous $NaHCO_3$ solution (1%, 5 mL) was added into it. The organic components were extracted into ethyl acetate, which was then dried over anhydrous Na_2SO_4. Evaporation of the solvent gave the crude product. The isolated yield was obtained by flash column chromatography on silica gel with petroleum ether/ethyl acetate = 12/1 as the eluent. The product was identified by ^1H NMR analysis. Under these conditions, a smooth reaction resulted that produced the corresponding α-amino nitrile in 95% yield. The same reaction conditions were used for testing the catalytic activity of complex **2**. The results are collected in Table 2.

As can be seen from Table 2, both **1** and **2** could promote the cyanosilylation reaction between trimethylsilyl cyanide with *N*-benzylidenebenzenamine (entry 1) and substituted imine (entries 2–10). In the absence of networks **1** and **2**, the reaction did not proceed at all, thereby supporting the possible Lewis acid catalyzed activity of the networks. Likewise, when the catalyst was filtered off, the reaction was no longer promoted. Further, a control experiment using $Cu(Ac)_2$ as the catalyst did not result in any product formation. These control experiments strongly suggest that the soluble and catalytically active species are not leached out from both networks. Thus, the reaction was promoted by heterogeneous catalysis of complexes **1** and **2**.

Notably, the heterogeneous catalysts can be conveniently recovered from the reaction mixture by simple filtration and used several times (tested four consecutive times; entry 1, Table 2) without much loss in the catalytic efficiency (4% drop in isolated yield in the fourth run). Moreover, the

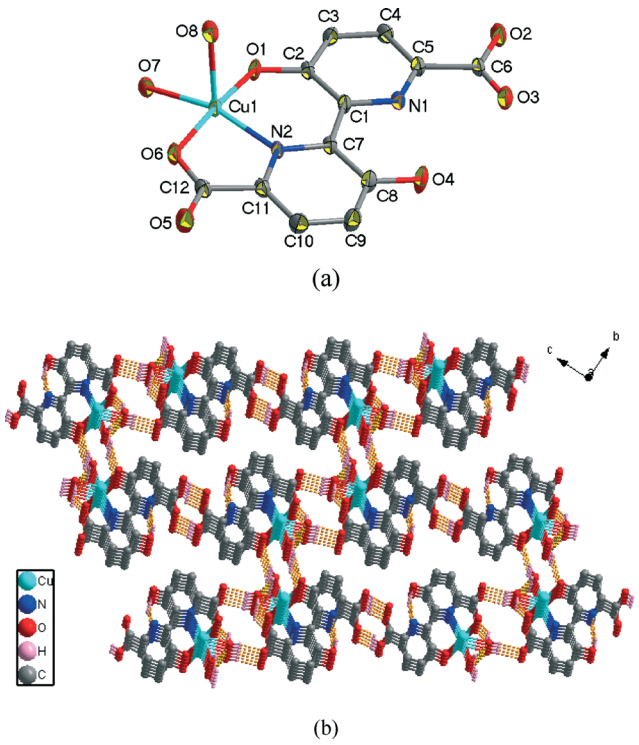

Fig. 4 (a) The coordination environment of the Cu(II) center in **5** with the ellipsoids drawn at the 50% probability level. The hydrogen atoms are omitted for clarity. (b) View of the 3D supramolecular network. The extensive hydrogen bonds are colored yellow.

recovered MOFs remained stable with complete retention of reactivity, which is further confirmed by PXRD analysis. As shown in Fig. S3 and S4,† the recovered material shows no change in the structure of the catalyst.

Magnetic properties

The magnetic susceptibility of powdered samples of complexes **1**, **2** and **4** was measured from 2 to 300 K under a constant magnetic field of 0.1 T.

Polymer **1** displays a strong antiferromagnetic interaction. The detailed discussion is reported in our previous paper.[14d]

The magnetic susceptibilities of **2** were measured in the 2–300 K temperature range, and shown as $\chi_M T$ and χ_M *versus* T plots in Fig. 5. The experimental $\chi_M T$ value of **2** at room temperature is 0.76 cm^3 K mol^{-1}, which is close to that expected for two uncoupled Cu(II) ions (0.75 cm^3 K mol^{-1}, S = 1/2). The temperature dependence of the reciprocal susceptibilities ($1/\chi_M$) of **2** obeys the Curie–Weiss law above 30 K with θ = −24.57 K, C = 0.89 cm^3 K mol^{-1}. As temperature is lowered to 2 K, the $\chi_M T$ values decrease first slowly and then rapidly. The behavior suggests that antiferromagnetic interactions are operative in **2**.

According to the structure of **2**, it could be presumed that the main magnetic interactions between the metal centers might happen between two carboxylate bridged Cu(II) ions (namely, between Cu1 and Cu2), whereas the superexchange interactions between Cu(II) ions (Cu2 and Cu2) through the $hbptc^{4-}$ ligand bridges can be ignored because of the

Table 2 Strecker reaction of trimethylsilyl cyanide with various imines

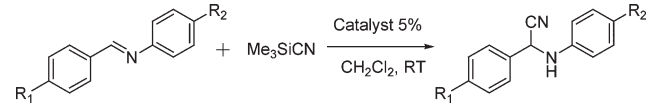

Entry	Imine	Yield[a] (%) 1	2
1	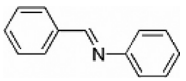	95, 93,[b] 91[c]	93, 91,[b] 89[c]
2	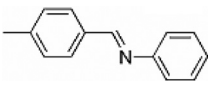	95	93
3	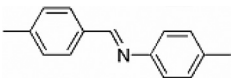	93	91
4	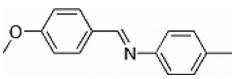	92	91
5	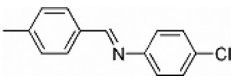	94	92
6	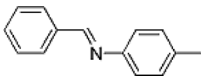	93	90
7	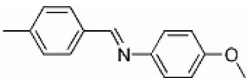	92	90
8	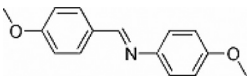	92	91
9	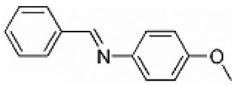	94	92
10	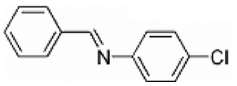	94	93

[a] Yield based on column chromatography. [b] Isolated yield after the third and fourth run. [c] Isolated yield after the third and fourth run.

long length of the $hbpdc^{4-}$ ligands. Therefore, the analysis of the susceptibility curves was performed using the Bleaney–Bowers formula[27] with the exchange Hamiltonian ($H = -JS_1S_2$, $S_1 = S_2 = 1/2$)

$$\chi_M = (2N\beta^2g^2/kT)[3 + \exp(-J/kT)]^{-1}(1 - \rho) + (N\beta^2g^2/2kT)\rho + N_\alpha$$

Least-squares fitting of the experimental data led to J = −13.46 cm^{-1}, g = 2.04, ρ = 0.020, and $R = 2.2 \times 10^{-3}$ with R defined as $\sum(\mu_{obsd} - \mu_{calcd})^2/\sum(\mu_{obsd})^2$, where ρ is the percentage of the paramagnetic impurities, N_α the temperature-independent paramagnetism (120×10^{-6} cm^3 mol^{-1}), and N, β and k have their usual meanings. The curve calculated with these parameters gave a reasonable fit to the experimental data as shown by the solid line in Fig. 5.

The magnetic properties of complex **4** under the form of the $\chi_M T$ and χ_M *versus* T plot are shown in Fig. 6. The experimental $\chi_M T$ value of **4** at room temperature is 0.77 cm^3 K mol^{-1}, which is close to that expected for two uncoupled Cu(II) ions

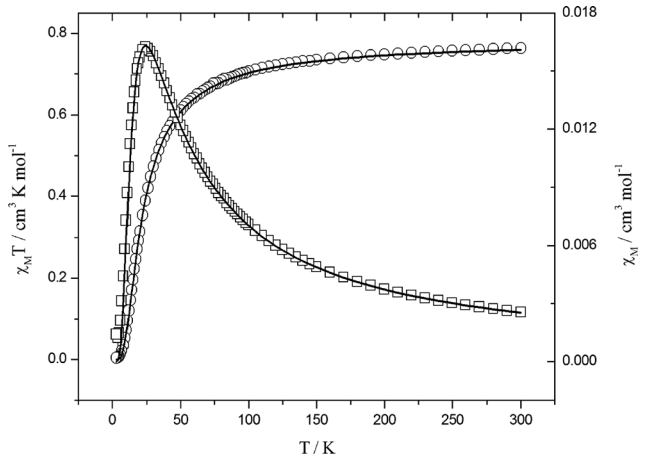

Fig. 5 Temperature dependence of $\chi_M T$ and χ_M for **2**. Open points are the experimental data, and the solid line represents the best fit obtained from the Hamiltonian given in the text.

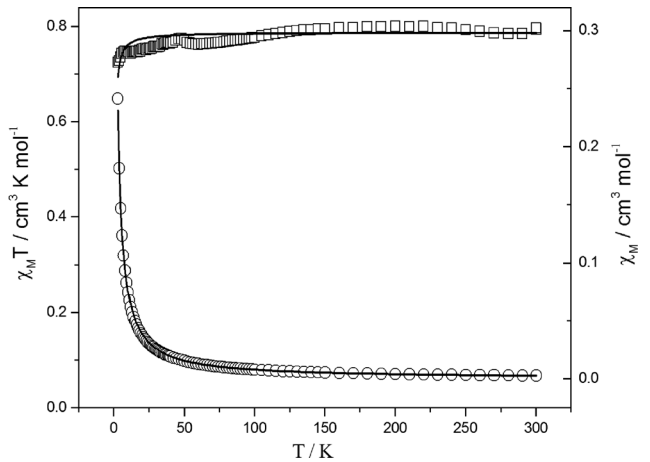

Fig. 6 Temperature dependence of $\chi_M T$ and χ_M for **4**. Open points are the experimental data, and the solid line represents the best fit obtained from the Hamiltonian given in the text.

(0.75 cm^3 K mol^{-1}). Upon cooling, the $\chi_M T$ values remain almost constant up to 100 K, and then decreases at lower temperatures, thus complex **4** displays overall weak antiferromagnetic coupling. The crystal structure of **4** is made up of a double-stranded dimer and thus the magnetic susceptibility data can be analyzed by means of the Bleaney–Bowers equation for a copper(II) dimer.[27] The spin Hamiltonian is defined as $H = -J(S_1S_2)$.

$$\chi_M = (Ng^2\beta^2/3KT)[6/(3 + \exp(-J/kT))]$$

The best least-squares fit parameters are g = 2.050 (2), J = −0.457(1) cm^{-1}, and $R = 7.285 \times 10^{-4}$. The small J value indicates a weak antiferromagnetic interaction between the dimers.

Conclusions

In conclusion, we have carried out *in situ* generation of another functionality with a rigid $mbptcH_2$ ligand under hydrothermal conditions to assemble five multi-functional copper(II) complexes. By fine tuning the reactant ratio and reaction temperature, 3D, 2D, and 0D complexes can be acquired. Such slight modifications in the reaction conditions affect strongly the composition and structure of the obtained complexes.

Complex **1** exhibits very strong antiferromagnetic interactions, while complexes **2** and **4** display weak antiferromagnetic interactions. In **2**, the relative configuration of the $hbpdcH_4$ ligand with respect to the magnetic orbitals offers a poor overlap between them, while in complex **4** it is due to the lack of a magnetic exchange pathway, which can be clearly seen from the structural plot.

The catalytic results reveal that complexes **1** and **2**, featuring Lewis acid-type catalytic sites, can function as heterogeneous, very efficient and reusable catalysts for the Strecker reaction of imines.

Acknowledgements

We gratefully acknowledge financial support from the Natural Science Foundation of China (grant no. 21372112 and 21272109) and the Technology Innovation Team Support Programs of Henan Province University (no. 2012IRTSTHN019 and 14IRTSTHN008).

References

1 (*a*) B. Chen, S. Xiang and G. Dong, *Acc. Chem. Res.*, 2010, **43**, 1115–1124; (*b*) L. Ma, C. Abney and W. Lin, *Chem. Soc. Rev.*, 2009, **38**, 1248–1256; (*c*) M. D. Allendorf, C. A. Bauer, R. K. Bhakta and R. J. T. Houk, *Chem. Soc. Rev.*, 2009, **38**, 1330–1352; (*d*) O. R. Evans and W. B. Lin, *Acc. Chem. Res.*, 2002, **35**, 511–522.

2 (*a*) P. Mahata and S. Natarajan, *Chem. Soc. Rev.*, 2009, **38**, 2304–2318; (*b*) J. R. Li, R. J. Kuppler and H. C. Zhou, *Chem. Soc. Rev.*, 2009, **38**, 1477–1504; (*c*) Y. G. Huang, F. L. Jiang and M. C. Hong, *Coord. Chem. Rev.*, 2009, **253**, 2814–2834.

3 (*a*) D. Sarma, P. Mahata, S. Natarajan, P. Panissod, G. Rogez and M. Drillon, *Inorg. Chem.*, 2012, **51**, 4495–4501; (*b*) C. S. Liu, W. Guo, E. C. Sañudo, M. Chen, M. Hu, M. Du and S. M. Fang, *CrystEngComm*, 2012, **14**, 160–168; (*c*) T. F. Liu, J. Lü, C. B. Tian, M. N. Cao, Z. J. Lin and R. Cao, *Inorg. Chem.*, 2011, **50**, 2264–2271.

4 (*a*) Z. W. Wang, C. C. Ji, J. Li, Z. J. Guo, Y. Z. Li and H. G. Zheng, *Cryst. Growth Des.*, 2009, **9**, 475–482; (*b*) D. A. McMorran, *Inorg. Chem.*, 2008, **47**, 592–601; (*c*) P. Mahata and S. Natarajan, *Inorg. Chem.*, 2007, **46**, 1250–1258.

5 (*a*) A. Karmakar, H. M. Titi and I. Goldberg, *Cryst. Growth Des.*, 2011, **11**, 2621–2636; (*b*) D. Sun, H. R. Xu, C. F. Yang, Z. H. Wei, N. Zhang, R. B. Huang and L. S. Zheng, *Cryst. Growth Des.*, 2010, **10**, 4642–4649; (*c*) P. Mahata, D. Sen and S. Natarajan, *Chem. Commun.*, 2008, 1278–1280.

6 (*a*) F. Luo, Y. X. Che and J. M. Zheng, *Cryst. Growth Des.*, 2009, **9**, 1066–1071; (*b*) D. L. Reger, R. P. Watson and M. D. Smith, *Inorg. Chem.*, 2006, **45**, 10077–10087; (*c*) Y. Cui,

O. R. Evans, H. L. Ngo, P. S. White and W. B. Lin, *Angew. Chem., Int. Ed.*, 2002, **41**, 1159–1162.

7 (*a*) L. L. Liu, Z. G. Ren, L. W. Zhu, H. F. Wang, W. Y. Yan and J. P. Lang, *Cryst. Growth Des.*, 2011, **11**, 3479–3488; (*b*) J. X. Chen, X. Y. Tang, Y. Chen, W. H. Zhang, L. L. Li, R. X. Yuan, Y. Zhang and J. P. Lang, *Cryst. Growth Des.*, 2009, **9**, 1461–1469; (*c*) B. Zheng, H. Dong, J. F. Bai, Y. Li, S. Li and M. Scheer, *J. Am. Chem. Soc.*, 2008, **130**, 7778–7779.

8 (*a*) Y. Liu, Y. Qi, Y. H. Su, F. H. Zhao, Y. X. Che and J. M. Zheng, *CrystEngComm*, 2010, **12**, 3283–3290; (*b*) P. X. Yin, J. Zhang, Z. J. Li, Y. Y. Qin, J. K. Chen, L. Zhang, Q. P. Lin and Y. G. Yao, *Cryst. Growth Des.*, 2009, **9**, 4884–4896.

9 (*a*) H. X. Yang, S. Y. Gao, J. Lü, B. Xu, J. X. Lin and R. Cao, *Inorg. Chem.*, 2010, **49**, 736–744; (*b*) L. S. Long, *CrystEngComm*, 2010, **12**, 1354–1365; (*c*) B. X. Dong and Q. Xu, *Inorg. Chem.*, 2009, **48**, 5861–5873.

10 (*a*) K. L. Zhang, C. T. Hou, J. J. Song, Y. Deng, L. Li, S. W. Ng and G. W. Diao, *CrystEngComm*, 2012, **14**, 590–600; (*b*) F. Yu and B. Li, *CrystEngComm*, 2011, **13**, 7025–7031; (*c*) J. Zhang and X. H. Bu, *Chem. Commun.*, 2008, 444–446; (*d*) S. Bauer and N. Stock, *Angew. Chem., Int. Ed.*, 2007, **46**, 6857–6860.

11 (*a*) G. B. Li, J. M. Liu, Y. P. Cai and C. Y. Su, *Cryst. Growth Des.*, 2011, **11**, 2763–2772; (*b*) A. Lan, K. Li, H. Wu, D. H. Olson, T. J. Emge, W. Hong, M. Ki and J. Li, *Angew. Chem.*, 2009, **121**, 2370–2374; (*c*) S. Y. Lee, S. Park, H. J. Kim, J. H. Jung and S. S. Lee, *Inorg. Chem.*, 2008, **47**, 1913–1915.

12 (*a*) W. Y. Wang, Z. L. Yang, C. J. Wang, H. J. Lu, S. Q. Zang and G. Li, *CrystEngComm*, 2011, **13**, 4895–4902; (*b*) F. Luo, Y. X. Che and J. M. Zheng, *Cryst. Growth Des.*, 2009, **9**, 1066–1071; (*c*) Z. Pan, Y. Song, Y. Jiao, Z. Fang, Y. Li and H. Zheng, *Inorg. Chem.*, 2008, **47**, 5162–5168; (*d*) K. S. Gavrilenko, O. Cador, K. Bernot, P. Rosa, R. Sessoli, S. Golhen, V. V. Pavlishchuk and L. Ouahab, *Chem. – Eur. J.*, 2008, **14**, 2034–2043.

13 (*a*) S. L. Xiang, J. Huang, L. Li, J. Y. Zhang, L. Jiang, X. J. Kuang and C. Y. Su, *Inorg. Chem.*, 2011, **50**, 1743–1748; (*b*) P. Lama, A. Aijaz, E. C. Sanudo and P. K. Bharadwaj, *Cryst. Growth Des.*, 2010, **10**, 283–290; (*c*) X. C. Huang, W. Luo, Y. F. Shen, X. J. Lin and D. Li, *Chem. Commun.*, 2008, 993–995.

14 (*a*) T. Zhang, C. Spitz, M. Antonietti and C. F. J. Faul, *Chem. – Eur. J.*, 2005, **11**, 1001–1009; (*b*) J. Yang, Q. Yue, G. D. Li, J. J. Cao, G. H. Li and J. S. Chen, *Inorg. Chem.*, 2006, **45**, 2857–2865; (*c*) U. Dawid, F. P. Pruchnik and R. Starosta, *Dalton Trans.*, 2009, 3348–3353; (*d*) B. M. Ji, D. S. Deng, H. H. Lan, C. X. Du, S. L. Pan and B. Liu, *Cryst. Growth Des.*, 2010, **10**, 2851–2853; (*e*) B. M. Ji, D. S. Deng, X. He, B. Liu, S. B. Miao, N. Ma, W. Z. Wang, L. G. Ji, P. Liu and X. F. Li, *Inorg. Chem.*, 2012, **51**, 2170–2177.

15 (*a*) Y. H. Liu, Y. L. Lu, H. C. Wu, J. C. Wang and K. L. Lu, *Inorg. Chem.*, 2002, **41**, 2592–2597; (*b*) D. Bradshaw, J. B. Claridge, E. J. Cussen, T. J. Prior and M. J. Rosseinsky, *Acc. Chem. Res.*, 2005, **38**, 273–282; (*c*) J. Y. Wu, T. T. Yeh, Y. S. Wen, J. Twu and K. L. Lu, *Cryst. Growth Des.*, 2006, **6**, 467–473; (*d*) N. R. Kelly, S. Goetz, S. R. Batten and P. E. Kruger, *CrystEngComm*, 2008, **10**, 1018–1026.

16 (*a*) R. J. Kuppler, D. J. Timmons, Q. R. Fang, J. R. Li, T. A. Makal, M. D. Young, D. Q. Yuan, D. Zhao, W. J. Zhuang and H. C. Zhou, *Coord. Chem. Rev.*, 2009, **253**, 3042–3066; (*b*) D. J. Tranchemontagne, J. L. Mendoza-Cortes, M. O'Keeffe and O. M. Yaghi, *Chem. Soc. Rev.*, 2009, **38**, 1257–1283; (*d*) Z. Wang, G. Chen and K. L. Ding, *Chem. Rev.*, 2009, **109**, 322–359.

17 (*a*) K. Ohara, M. Kawano, Y. Inokuma and M. Fujita, *J. Am. Chem. Soc.*, 2010, **132**, 30–31; (*b*) A. Corma, H. Garcia and F. X. L. Xamena, *Chem. Rev.*, 2010, **110**, 4606–4655; (*c*) T. Uemura, Y. Ono, Y. Hijikata and S. Kitagawa, *J. Am. Chem. Soc.*, 2010, **132**, 4917–4924; (*d*) A. P. Singh, G. Kumar and R. Gupta, *Dalton Trans.*, 2011, **40**, 12454–12461; (*e*) G. Kumar and R. Gupta, *Inorg. Chem.*, 2012, **51**, 5497–5499.

18 *SHELXTL, Version 5.1*, Bruker AXS: Madison, WI, 1998.

19 G. M. Sheldrick, *SHELXS-97 and SHELXL-97, Program for X-ray Crystal Structure Solution*, University of Göettingen, Germany, 1997.

20 (*a*) H. B. Zhu and S. H. Gou, *Coord. Chem. Rev.*, 2011, **255**, 318–338; (*b*) H. Zhao, Z. R. Qu, H. Y. Ye and R. G. Xiong, *Chem. Soc. Rev.*, 2008, **37**, 84–100; (*c*) X. M. Chen and M. L. Tong, *Acc. Chem. Res.*, 2007, **40**, 162–170.

21 (*a*) D. S. Li, P. Zhang, J. Zhao, Z. F. Fang, M. Du, K. Zou and Y. Q. Mu, *Cryst. Growth Des.*, 2012, **12**, 1697–1702; (*b*) Y. P. Wu, D. S. Li, F. Fu, W. W. Dong, J. Zhao, K. Zou and Y. Y. Wang, *Cryst. Growth Des.*, 2011, **11**, 3850–3857; (*c*) E. Nauha, A. Ojala, M. Nissinen and H. Saxell, *CrystEngComm*, 2011, **13**, 4956–4964.

22 (*a*) D. S. Deng, L. L. Liu, B. M. Ji, G. J. Yin and C. X. Du, *Cryst. Growth Des.*, 2012, **12**, 5338–5348; (*b*) Z. G. Li, G. H. Wang, H. Q. Jia, N. H. Hu and J. W. Xu, *CrystEngComm*, 2007, **9**, 882–887.

23 (*a*) J. Boonmak, S. Youngme, N. Chaichit, G. A. van Albada and J. Reedijk, *Cryst. Growth Des.*, 2009, **9**, 3318–3326; (*b*) Y. Y. Karabach, A. M. Kirillov, M. Haukka, J. Sanchiz, M. N. Kopylovich and A. J. L. Pombeiro, *Cryst. Growth Des.*, 2008, **8**, 4100–4108.

24 (*a*) A. H. Yang, H. Zhang, H. L. Gao, W. Q. Zhang, L. He and J. Z. Cui, *Cryst. Growth Des.*, 2008, **8**, 3354–3359; (*b*) U. Mukhopadhyay and I. Bernal, *Cryst. Growth Des.*, 2006, **6**, 363–365.

25 (*a*) H. X. Li, W. Zhao, H. Y. Li, Z. L. Xu, W. X. Wang and J. P. Lang, *Chem. Commun.*, 2013, **49**, 4259–4261; (*b*) Z. Q. Xu, Q. Wang, H. J. Li, W. Meng, Y. Han, H. W. Hou and Y. T. Fan, *Chem. Commun.*, 2012, **48**, 5736–5738; (*c*) I. H. Hwang, J. M. Bae, W. S. Kim, Y. D. Jo, C. Kim, Y. Kim, S. J. Kim and S. Huh, *Dalton Trans.*, 2012, **41**, 12759–12765.

26 (*a*) A. M. Seayad, B. Ramalingam, K. Yoshinaga, T. Nagata and C. L. L. Chai, *Org. Lett.*, 2010, **12**, 264–267; (*b*) M. Hatano, Y. Hattori, Y. Furuya and K. Ishihara, *Org. Lett.*, 2009, **11**, 2321–2324; (*c*) J. Jarusiewicz, Y. Choe, K. S. Yoo, C. P. Park and K. W. Jung, *J. Org. Chem.*, 2009, **74**, 2873–2876; (*d*) R. Reingruber, T. Baumann, S. Dahmen and S. Broese, *Adv. Synth. Catal.*, 2009, **351**, 1019–1024.

27 O. Kahn, *Molecular Magnetism*, VCH Publishers, New York, 1993.

